A Parameterization of Interstitial Aerosol Extinction and Its Application to Marine Cloud Brightening

FABIAN HOFFMANN,[a] BERNHARD MAYER,[a] AND GRAHAM FEINGOLD[b]

[a] *Meteorologisches Institut, Ludwig-Maximilans-Universität München, Munich, Germany*
[b] *Chemical Sciences Laboratory, NOAA/Earth System Research Laboratories, Boulder, Colorado*

(Manuscript received 21 February 2022, in final form 8 June 2022)

ABSTRACT: Marine cloud brightening (MCB) is a geoengineering approach to counteract climate change by the deliberate seeding of sea salt aerosol particles that, once they activated to cloud droplets, directly increase cloud reflectance and hence global albedo. However, a large fraction of the seeded aerosol may remain interstitial, i.e., unactivated particles among cloud droplets. Because the consideration of interstitial aerosol optical properties usually requires computationally expensive simulations of the entire particle spectrum and direct Mie calculations, we develop a simple parameterization to be used with computationally efficient bulk and even bin cloud microphysical schemes that do not treat the unactivated aerosol explicitly. Using parcel and large-eddy simulations with highly detailed Lagrangian cloud microphysics and direct Mie calculations as a reference, we show that the parameterization captures the variability in the interstitial aerosol extinction successfully. By applying the parameterization to typical MCB cases, we find that the consideration of interstitial aerosol extinction is important for the assessment of MCB in shallow clouds with weak updrafts, in which only a small fraction of aerosol particles is activated to cloud droplets.

SIGNIFICANCE STATEMENT: The optical properties of clouds are not only determined by the number and size of cloud droplets. Unactivated aerosol particles, so-called interstitial aerosol, can contribute substantially to the optical thickness of shallow clouds with weak updrafts in aerosol-laden conditions. The consideration of interstitial aerosol optical thickness has been computationally challenging, but the new parameterization presented here allows for an efficient representation in various types of cloud models. The parameterization is shown to be an important addition for the assessment of marine cloud brightening (MCB), a potential geoengineering technique to counteract global warming by increasing the cloud albedo through the deliberate seeding of aerosol.

KEYWORDS: Cloud droplets; Cloud forcing; Cloud microphysics; Cloud radiative effects; Cloud seeding; Aerosol-cloud interaction

1. Introduction

As global temperatures rise and impacts on mankind, society, and the environment become increasingly obvious, the demand for more immediate ways to counteract climate change is rising (e.g., Victor et al. 2014; Gulev et al. 2021). Under the umbrella of geoengineering, several techniques have been proposed to counteract global warming by either directly removing carbon dioxide from the atmosphere or altering Earth's radiation budget (e.g., Vaughan and Lenton 2011).

One of the latter approaches is marine cloud brightening (MCB) (Latham and Smith 1990; Latham et al. 2012; Diamond et al. 2022), in which seawater is sprayed into the atmosphere where it evaporates and leaves sea salt aerosol particles that may act as the condensation nuclei for additional cloud droplets. These additional cloud droplets tend to increase the cloud albedo and hence increase the amount of solar shortwave radiation that is reflected back to space, ultimately cooling the atmosphere (e.g., Twomey 1974).

A recent study has shown that the success of MCB depends crucially on the number and size of the sprayed seawater droplets, forming the seeded aerosol size distribution after evaporation (Hoffmann and Feingold 2021): Aerosol particles that are too large may accelerate the precipitation process and therefore cause a premature dissipation of the cloud deck. Too many (small) aerosol particles may accelerate the evaporation of cloud water at cloud top, increasing the mixing with the free troposphere and also dissipating the cloud deck prematurely. Furthermore, the aerosol size distribution is constrained by the energy required to pump and disperse seawater into the atmosphere. As initially discussed by Connolly et al. (2014), the required energy is primarily determined by the flux of seawater sprayed into the atmosphere. As the cloud albedo increases with the droplet number, this constraint favors seeding smaller aerosol sizes. Aerosol particles that are too small, however, do not necessarily activate to cloud droplets, leaving a large fraction of seeded aerosol particles as interstitial aerosol. Based on these arguments, Connolly et al. (2014) suggested dry aerosol particles in the radius range between 15 and 50 nm are optimal for MCB, which was later confirmed by Wood (2021). Wood (2021) also showed that increasing the background cloud droplet concentration by at least a factor of 3 through MCB is sufficient to offset global warming, which might require increasing the droplet concentration in the preferentially targeted stratocumulus regions to values between 300 and 1000 cm^{-3}.

Corresponding author: Fabian Hoffmann, fa.hoffmann@lmu.de

DOI: 10.1175/JAS-D-22-0047.1

By adding these large numbers of aerosol particles, the contribution of interstitial aerosol to the optical thickness and hence the albedo of clouds targeted in MCB can be substantial. Connolly et al. (2014) and Hoffmann and Feingold (2021) showed this using sophisticated cloud microphysical models that represent the entire hydrometeor size distribution, including interstitial aerosol particles. Simpler and therefore computationally inexpensive cloud microphysical models often neglect this part of the hydrometeor spectrum. Additionally, a detailed radiative transfer code that includes Mie scattering needs to be applied for determining the optical thickness of interstitial aerosol particles, as these often exhibit sizes close to the wavelength of the shortwave radiation they interact with, prohibiting the commonly applied, simple geometric scattering approximation valid for larger cloud droplets. The commensurately high computational requirements make the application of these modeling frameworks to larger domains and longer time spans difficult (e.g., Nussenzveig and Wiscombe 1980). However, we need these comprehensive assessments to determine the potentials and risks of MCB, as the natural variability of meteorological and background aerosol conditions is insufficiently represented in idealized case studies (e.g., Glassmeier et al. 2021).

Therefore, in this study, we develop a parameterization for the interstitial aerosol thickness to be used with bulk microphysical schemes and even more comprehensive bin models that neglect the explicit representation of (interstitial) aerosol particles. Also models that represent interstitial aerosol can benefit from a computationally efficient estimate of the interstitial aerosol optical thickness through the parameterization. We validate the parameterization with highly detailed cloud microphysical simulations using a Lagrangian cloud model (Hoffmann et al. 2015, 2019) and an accurate Mie radiative transfer code (Wiscombe 1980). Finally, we apply the parameterization to identify conditions under which this parameterization has significant impact on MCB. Based on these objectives, the paper is organized as follows. In the following section (section 2), we will derive the parameterization, and verify it subsequently (section 3). The parameterization is applied in an MCB scenario in section 4, and we conclude the paper with a summary (section 5).

2. Parameterization development

The primary target of MCB is increasing the cloud albedo A_c. According to Meador and Weaver (1980), the two-stream approximation solution for A_c is

$$A_c = \frac{(1-g)\tau_c}{2+(1-g)\tau_c}, \tag{1}$$

where $g \approx 0.85$ is the scattering asymmetry parameter, i.e., the degree of forward scattering, which decreases slightly for smaller droplets and aerosol particles, as further discussed in the appendix. The cloud optical thickness τ_c is defined as

$$\tau_c(\lambda) = \int_{z_b}^{z_t} \left[\int_0^{\infty} Q_{\text{ext}}(r,\lambda)\pi r^2 n(r,z)dr \right] dz \tag{2}$$

$$= \int_{z_b}^{z_t} [\beta_{\text{ext},a}(\lambda,z) + \beta_{\text{ext},c}(\lambda,z)]dz, \tag{3}$$

which is the vertically integrated hydrometeor surface area distribution, where $n(r, z)dr$ is the number concentration of hydrometeors of size r at height z. The distribution is weighted by the extinction efficiency $Q_{\text{ext}}(r, \lambda)$, which is a function of the hydrometeor radius r and the wavelength of the scattered radiation, λ. Unless stated otherwise, we assume $\lambda = 500$ nm in the following, being representative for the bulk of solar shortwave radiation. The lower and upper bounds of the integral, z_b and z_t, are the cloud-base and cloud-top heights, respectively. By separating the hydrometeor distribution into aerosol particles and cloud droplets, as is usually done by applying Köhler theory (Köhler 1936) or defining a fixed separation radius on the order of 1 μm, one can determine the extinction caused by each species, $\beta_{\text{ext},a}$ and $\beta_{\text{ext},c}$, respectively.

The extinction by cloud droplets is often approximated as

$$\beta_{\text{ext},c} = \frac{3}{4}\frac{q_l}{\rho_l r_{\text{eff},c}} Q_{\text{ext}}^{\text{geo}}, \tag{4}$$

where $Q_{\text{ext}}^{\text{geo}} = 2$ is the extinction efficiency in the limit of geometric scattering ($2\pi r \gg \lambda$), q_l the liquid water content, ρ_l the mass density of water, and $r_{\text{eff},c}$ the cloud droplet effective radius which can often be expressed as a function of the volume mean radius (e.g., Freud and Rosenfeld 2012). Determining $\beta_{\text{ext},a}$ is, however, more complicated because $2\pi r \approx \lambda$, which requires the consideration of Mie theory for Q_{ext} (black line in Fig. 1). While there are several approximations to represent the extinction of aerosol particles in subsaturated, noncloudy environments (e.g., Shettle and Fenn 1979; Khvorostyanov and Curry 1999, 2007), there is only a limited number of attempts to parameterize $\beta_{\text{ext},a}$ for interstitial aerosol (Ghan et al. 2001).

The size of the interstitial aerosol particles can be derived from Köhler theory. As these particles are not activated, they tend to grow by the diffusion of water molecules until they assume a particle size that is in equilibrium with their environment. Sedunov (1974) derived exact expressions for this equilibrium radius in sub- and supersaturated conditions. Unfortunately, these solutions involve trigonometric and hyperbolic functions that make the subsequent derivations more complicated, if not impossible. Thus, for this study, we assume that the cloud is exactly saturated, which allows us to determine the equilibrium radius as

$$r_{\text{equi}} = \left(\frac{\text{br}_a^3}{A}\right)^{1/2}, \tag{5}$$

where r_a is the dry aerosol radius, and $b = \nu\rho_a m_l/(\rho_l m_a)$ and $A = 2\sigma/(\rho_l R_v T)$ represent the Köhler coefficients for the solute (Raoult) and curvature (Kelvin) effect, respectively. ν is the van't Hoff factor, ρ_a aerosol mass density, m_a and m_l molecular weights of the aerosol and liquid water, respectively, σ surface tension of the air–liquid water surface, R_v specific gas constant of water vapor, and T temperature. Assuming saturated conditions is a reasonable assumption for the clouds

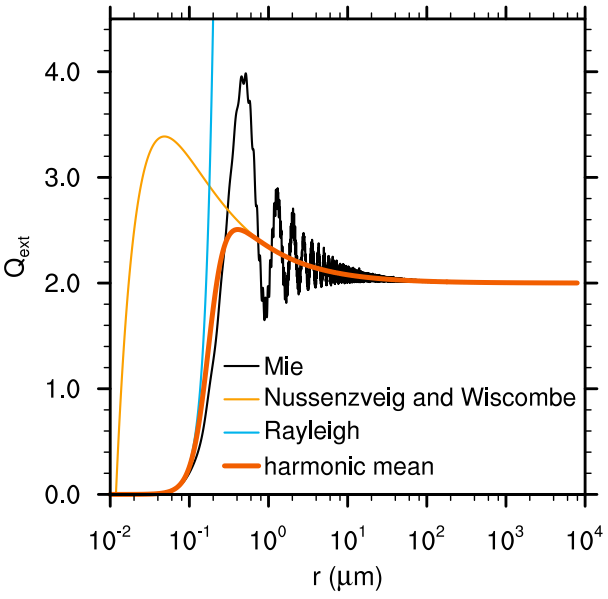

FIG. 1. The extinction efficiency Q_{ext} as a function of the radius of a liquid water sphere, derived from direct Mie theory (black line), the Nussenzveig and Wiscombe (1980) large-particle approximation of Mie scattering (yellow line), Rayleigh scattering (blue line), and a harmonic mean of the two aforementioned (orange line).

targeted in MCB, where the cloud droplet concentration is increased to several hundred cm^{-3} (Wood 2021), causing fast condensation of all excess water vapor. Furthermore, Mordy (1959) and Ivanova et al. (1977) showed that small aerosol particles reach their equilibrium size quickly after entering the cloud (<1 s), as is the case for the suggested size range of MCB aerosol particles between 15 and 50 nm in dry radius. Only larger particles ($r_a > 100$ nm) tend to require a longer time to assume their equilibrium size (Ivanova et al. 1977).

The distribution of r_a and hence r_{equi} can be represented by a lognormal distribution,

$$n_a(r_a) \equiv \frac{dN_a(r_a)}{dr_a} = \frac{N_a}{r_a \ln(\sigma_a)\sqrt{2\pi}} \exp\left[-\frac{\ln(r_a/r_{a,\text{mean}})^2}{2\ln(\sigma_a)^2}\right], \quad (6)$$

which natural and MCB aerosols often follow (e.g., Jaenicke 1993; Cooper et al. 2014). Here, $n_a(r_a)dr_a = dN_a(r_a)$ represents the (fractional) number concentration of aerosol particles with a r_a between r_a and $r_a + dr_a$. The lognormal distribution is specified by the (total) aerosol number concentration $N_a = \int_0^\infty n(r_a)dr_a$, geometric mean radius $r_{a,\text{mean}}$, and geometric (relative) standard deviation σ_a.

Considering Mie scattering for Q_{ext} in a simple, analytical form is difficult. The parameterization of Mitchell (2000) would be sufficient, but does not allow for the desired analytical consideration of lognormally distributed aerosol particles. The approximation of Nussenzveig and Wiscombe (1980) can be used in combination with lognormally distributed aerosol particles, and even successfully captures Mie scattering effects on Q_{ext} for large particles ($2\pi r \geq \lambda$), but overestimates Q_{ext} in the Rayleigh scattering regime ($2\pi r \ll \lambda$). Thus, we combine the Mie scattering approximation by Nussenzveig and Wiscombe (1980) with the description of Rayleigh scattering (e.g., Jacobson 2005) as the harmonic mean of both, as previously done by Jung and Kim (2007). Figure 1 shows that the harmonic mean offsets the deviations of its components for small and large particles, respectively, while it lacks the oscillations caused by Mie scattering that are usually lost when Q_{ext} is averaged over a distribution of particles. Based upon this observation, Jung and Kim (2007) expressed the extinction of dry aerosol particles as the harmonic mean of the extinction in each regime, which we adapt for interstitial aerosol particles as

$$\beta_{\text{ext},a} = \frac{\beta_{\text{ext},R}\beta_{\text{ext,NW}}}{\beta_{\text{ext},R} + \beta_{\text{ext,NW}}}, \quad (7)$$

where $\beta_{\text{ext},R} = \varphi_R M_{a,6}$ represents the extinction by Rayleigh scattering (e.g., Jacobson 2005) and $\beta_{\text{ext,NW}} = \varphi_{\text{NW1}} M_{a,2} + \varphi_{\text{NW2}} M_{a,4/3} + \varphi_{\text{NW3}} M_{a,2/3}$ the extinction by Mie scattering of large particles as approximated by Nussenzveig and Wiscombe (1980), with $M_{a,k}$ the kth moment of the assumed particle radius distribution. The coefficients are defined as $\varphi_R = (8/3)(2\pi/\lambda)^4[(n^2 - 1)/(n^2 + 2)]^2\pi$, $\varphi_{\text{NW1}} = 2\pi$, $\varphi_{\text{NW2}} = 1.992\,386\,1(2\pi/\lambda)^{-2/3}\pi$, and $\varphi_{\text{NW3}} = -0.715\,353\,7(2\pi/\lambda)^{-4/3}\pi$, with n being the (real) refractive index. Note that we include more terms from Nussenzveig and Wiscombe (1980) than initially done by Jung and Kim (2007), as these terms tend to result in a better agreement with the Mie reference, especially for smaller particles (not shown).

Note further that $\beta_{\text{ext},a}$ is calculated for the n of pure water in the following, while we neglect absorption, as is frequently done for the interaction of shortwave radiation and pure water. While solute aerosol can impact the refractive index of wetted aerosol particles and usually increases absorption, this effect is rather small for most types of water-soluble aerosol species (e.g., Tang 1997; Jacobson 2005). In fact, the aerosol mass constitutes only a few percent of the total particle mass at the assumed equilibrium size, (5), causing the optical properties of interstitial aerosol to be very similar to those of pure water. Thus, potential impacts of the solute aerosol on n are neglected. The consideration of absorption is, however, possible by including additional terms in (7).

For interstitial aerosol, we need to express $M_{a,k}$ by the truncated equilibrium radius distribution, with the dry aerosol radius of the largest interstitial aerosol particle, $r_{a,\text{crit}}$, as the upper limit. Hence,

$$\begin{aligned} M_{a,k}(r_{a,\text{crit}}) &= \int_0^{r_{a,\text{crit}}} r_{\text{equi}}(r_a)^k n_a(r_a) dr_a \\ &= \frac{N_a}{2} \exp\left[\frac{\left(\frac{3}{2}k\right)^2}{2} \ln(\sigma_a)^2\right] r_{\text{equi}}(r_{a,\text{mean}})^k \\ &\quad \times \left\{1 - \text{erf}\left[\frac{\left(\frac{3}{2}k\right)\ln(\sigma_a)^2 - \ln\left(\frac{r_{a,\text{crit}}}{r_{a,\text{mean}}}\right)}{\sqrt{2}\ln(\sigma_a)}\right]\right\}, \end{aligned} \quad (8)$$

where erf denotes the error function. The theoretical background for the derivation of (8) can be found in

Feingold and Levin (1986), with further references therein. By introducing the moments (8) into (7), we obtain the approximation for $\beta_{\text{ext},a}$ that will be used in the following. Larger particles with $r_a > r_{a,\text{crit}}$ are activated to cloud droplets, and their extinction can be determined using (4).

To account for a multimodal aerosol distribution, as is frequently the case for atmospheric aerosol (e.g., Jaenicke 1993), the contributions of each distribution can be estimated via (7), and the total interstitial aerosol extinction is determined by their sum

$$\beta_{\text{ext},a} = \sum_{k=1}^{K} \beta_{\text{ext},a,k}(r_{a,\text{crit},k}), \tag{9}$$

where $\beta_{\text{ext},a,k}$ and $r_{a,\text{crit},k}$ can be different for each mode. Differences in $r_{a,\text{crit},k}$ are due to differences in the chemical composition of each aerosol mode that result in the activation of smaller and larger particles sizes, as discussed further below.

Figure 2 shows $\beta_{\text{ext},a}/N_a$ as a function of $r_{a,\text{crit}}$ for the new parameterization (7) (orange lines), as well as the full Mie solution calculated using the model of Wiscombe (1980) (black lines). The parameters of the displayed aerosol distributions are chosen to reflect the optimal range of aerosol sizes for MCB with values of $r_{a,\text{mean}}$ ranging from 15 to 50 nm. For most plots, a distribution width of $\sigma_a = 2$ is chosen, which is typical for today's spraying apparatus (Cooper et al. 2014). A smaller width of $\sigma_a = 1.05$ is also analyzed, as some authors argue that a narrower distribution is worth aspiring to (e.g., Salter et al. 2008). A liquid water refractive index of $n = 1.334$ is prescribed, corresponding to the assumed wavelength of $\lambda = 500$ nm (e.g., Hale and Querry 1973). Note that all plots are normalized by N_a, with which $\beta_{\text{ext},a}$ scales linearly.

All panels of Fig. 2 show that $\beta_{\text{ext},a}$ increases with $r_{a,\text{crit}}$ due to an increasing number of aerosol particles contributing to the extinction. Note that the increase of $\beta_{\text{ext},a}$ is primarily determined by its dependency on r^2 [cf. (2)], and is therefore not clearly related to $r_{a,\text{mean}}$. Only narrow aerosol distributions (Fig. 2d) show a rather instantaneous increase in $\beta_{\text{ext},a}$ when $r_{a,\text{mean}}$ is exceeded. For large and broad aerosol distributions (Figs. 2b,c), the parameterization agrees well with the Mie reference in shape and absolute value. For small aerosols (Fig. 2a) and narrow distributions (Fig. 2d), the shape of $\beta_{\text{ext},a}$ is captured, but the absolute value deviates by up to 30%. In both cases, the absolute width of the aerosol distribution, $\sigma_a r_{a,\text{mean}}$, is rather narrow, making the parameterization of $\beta_{\text{ext},a}$ more susceptible to the oscillations of Mie scattering that are not captured in the parameterization (cf. black and orange lines in Fig. 1).

An essential step to apply the parameterization of $\beta_{\text{ext},a}$ in bulk and bin microphysical simulations is to back-calculate $r_{a,\text{crit}}$. Bulk and bin models usually apply a parameterization that predicts the concentration of cloud droplets, N_c, for a maximum supersaturation $S_{\max}$ that is typically reached at cloud base,

$$N_c = f_{\text{acti}}(S_{\max}), \tag{10}$$

where f_{acti} is the activation parameterization. Because many models do not predict supersaturation explicitly, $S_{\max}$ is often parameterized by the vertical velocity w, which, however, does not affect the following derivations. Abdul-Razzak et al. (1998) (further detailed in Abdul-Razzak and Ghan 2000, 2002) describe a frequently applied parameterization that can consider several modes of lognormally distributed aerosol particles with different physicochemical compositions as done here. Similar approaches have been suggested by, e.g., von der Emde and Wacker (1993) and Khvorostyanov and Curry (2006). Under the assumption that the concentration of cloud droplets is not changed by coalescence processes, it is possible to determine

$$S_{\max} = f_{\text{acti}}^{-1}(N_c), \tag{11}$$

where f_{acti}^{-1} is the inverse function of the activation parameterization. f_{acti}^{-1} can be obtained analytically for monomodal [see (31) in Abdul-Razzak et al. (1998)] and multimodal aerosol distributions [see (6) in Abdul-Razzak and Ghan (2000)]. [A numerical solution is also possible using the false position (regular falsi) root-finding algorithm that converges within a few iterations for this problem (Press et al. 1996, chapter 9.2).] As $S_{\max}$ is the same for all aerosol modes, one can determine an individual $r_{a,\text{crit},k}$ for each mode by equating $S_{\max}$ to the critical supersaturation according to Köhler theory,

$$S_{\max} = S_{\text{crit}} = \left(\frac{4A^3}{27 b_k r_{a,\text{crit},k}^3}\right)^{1/2}. \tag{12}$$

Note that due to b_k, which represents the chemical composition, $r_{a,\text{crit},k}$ can be different for each mode even if $S_{\max}$ is the same.

3. Verification

a. Comparison with Ghan et al. (2001)

We begin our verification by comparing our parameterization (7) to the aforementioned parameterization by Ghan et al. (2001), further detailed in Ghan and Zaveri (2007) and applied in Liu et al. (2012). We only repeat the most important parts of their parameterization here, and refer the reader to the aforementioned references for more details. In contrast to the truncated lognormal distributions used in our parameterization, their approach uses *full* lognormal distributions to describe the aerosol and wetted particle distribution in a two-moment bulk framework, predicting—inter alia—the dry aerosol number concentration N_a' and dry aerosol mass mixing ration q_a of a specific aerosol species. (Note that $N_a' = N_a - N_c \leq N_a$ due to the number of aerosol particles activated into cloud droplets.) By combining these quantities, the dry aerosol volume radius,

$$r_{a,\text{vol}} = \left(\frac{q_a \rho_{\text{air}}}{4/3\pi\rho_a N_a'}\right)^{1/3}, \tag{13}$$

is calculated, where ρ_{air} is the mass density of air. Ghan et al. (2001) use $r_{a,\text{vol}}$ to determine the corresponding wet radius through Köhler theory. For saturated conditions, this radius is identical to our r_{equi}. By applying the same σ_a for the dry aerosol and wetted particle distribution, as we also do, the corresponding wet surface mode radius is calculated as

$$r_{\text{equi,mean}} = r_{\text{equi}}(r_{a,\text{vol}})\exp\left[\frac{1}{2}\ln(\sigma_a)^2\right], \tag{14}$$

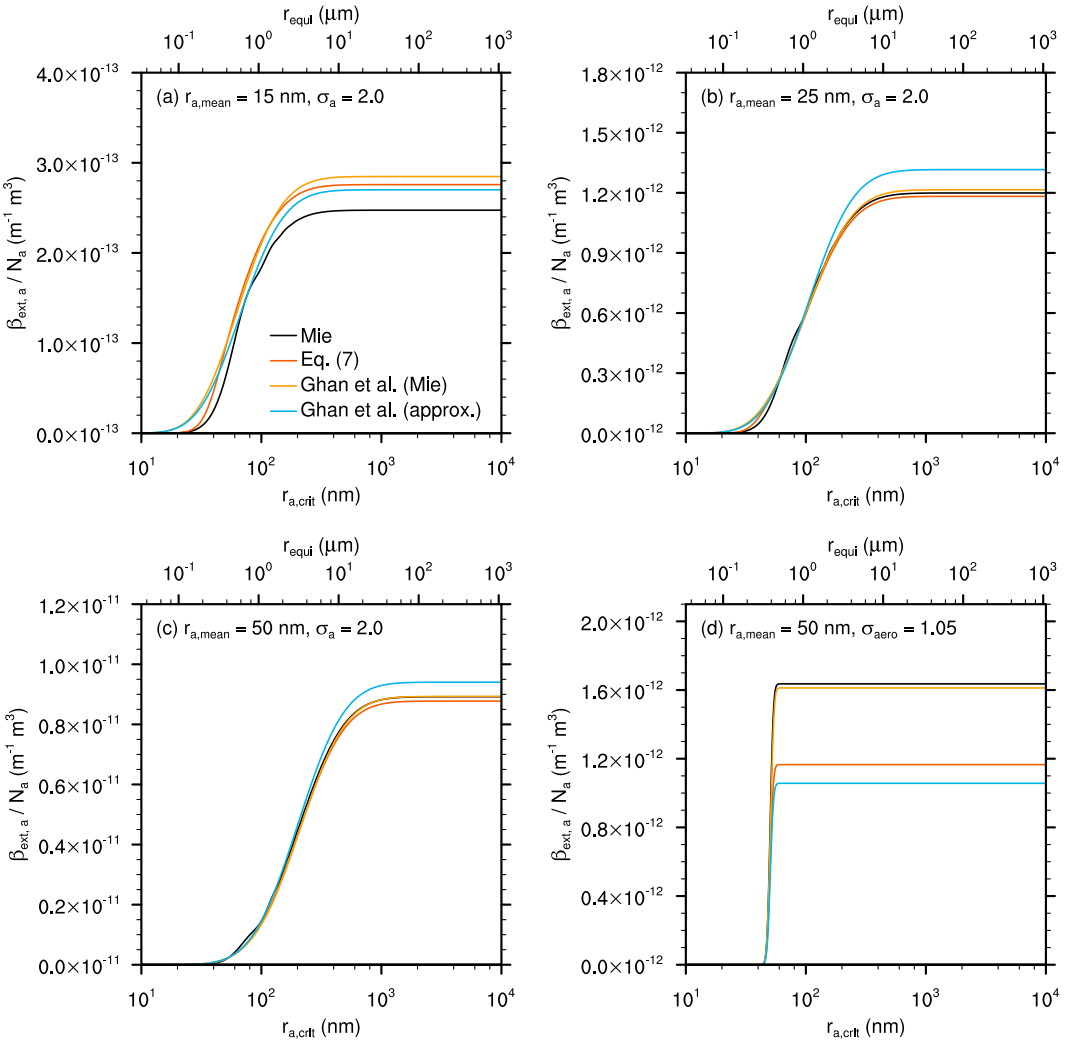

FIG. 2. The extinction $\beta_{\text{ext},a}$ normalized by the aerosol concentration N_a as a function of the $r_{a,\text{crit}}$, up to which the aerosol particles are assumed to contribute to $\beta_{\text{ext},a}$. Results are derived from Mie theory (black line) and the approximation (7) (orange line) for different aerosol distributions as indicated in the plot. Additionally, results from the parameterization by Ghan et al. (2001) are shown (yellow and blue lines), and discussed in section 3.

which is used as the geometric mean radius of the wetted aerosol distribution.

For the following verification, we determine the extinction as

$$\beta_{\text{ext},a}^{\text{Ghan}} = \overline{Q_{\text{ext}}}\,\pi r_{\text{equi}}(r_{a,\text{vol}})^2 N'_a, \tag{15}$$

which is analogous to the approach described in (12) of Ghan et al. (2001). Here, $\overline{Q_{\text{ext}}}$ is the surface-area weighted extinction coefficient of the assumed particle distribution, determined through σ_a and $r_{a,\text{vol}}$ via $r_{\text{equi,mean}}$. Ghan et al. (2001) suggest approximating $\overline{Q_{\text{ext}}}$ using fourth-order Chebyshev polynomials for computational efficiency. Additionally, we will determine $\overline{Q_{\text{ext}}}$ from Mie calculations directly to highlight some fundamental differences between the two parameterizations. Note that the same n and λ as in our parameterization are used to facilitate comparison. The results are shown in the previously introduced Fig. 2, depicting β_{ext}/N_a as a function of $r_{a,\text{crit}}$. To apply the parameterization by Ghan et al. (2001) and determine (13), we calculate the zeroth and third truncated moment of the dry aerosol size distribution,

$$\begin{aligned} M'_{a,k}(r_{a,\text{crit}}) &= \int_0^{r_{a,\text{crit}}} r_a^k n_a(r_a) dr_a \\ &= \frac{N_a}{2} \exp\left[\frac{k^2}{2} \ln(\sigma_a)^2\right] r_{a,\text{mean}}^k \\ &\quad \times \left\{1 - \text{erf}\left[\frac{k\ln(\sigma_a)^2 - \ln\left(\frac{r_{a,\text{crit}}}{r_{a,\text{mean}}}\right)}{\sqrt{2}\ln(\sigma_a)}\right]\right\}, \end{aligned} \tag{16}$$

to which N'_a and q_a are proportional.

We will discuss the parameterization by Ghan et al. (2001) with $\overline{Q_{\text{ext}}}$ from direct Mie calculations first. In this case, the

parameterization (yellow lines) captures the behavior of the Mie reference (black lines) well, especially when $r_{a,\mathrm{mean}}$ is large (Figs. 2b–d). For the smallest analyzed $r_{a,\mathrm{mean}}$ (Fig. 2a), similar deviations from the Mie reference as in the case of our parameterization occur. These deviations may be due to inherent uncertainties in the estimation of the correct mean size of the wetted particle distribution carried out in Ghan et al. (2001) via (13) and (14). Most interesting is that β_{ext}/N_a is overestimated by the Ghan et al. (2001) parameterization when a large fraction of aerosol particles is activated to cloud droplets, i.e., at small $r_{a,\mathrm{crit}}$ (best visible in Figs. 2a and 2b). The reason for this are the *full* lognormal distributions assumed in Ghan et al. (2001) that are not able to represent the instantaneous decrease in particles contributing to the extinction at $r_{a,\mathrm{crit}}$, which is better captured by the truncated lognormal particle spectra used in our parameterization (orange lines).

With $\overline{Q_{\mathrm{ext}}}$ from Mie calculations, the parameterization by Ghan et al. (2001) clearly exceeds the accuracy of our parameterization for narrow particle size distributions (yellow and orange lines in Fig. 2d). However, this is only due to the inherent smoothing of Q_{ext} in our parameterization, which does not allow one to capture the high-frequent oscillations of Mie scattering. This becomes obvious when $\overline{Q_{\mathrm{ext}}}$ is approximated by Chebyshev polynomials, as originally suggested by Ghan et al. (2001) (blue lines in Fig. 2). Due to the approximation, deviations from the Mie reference (black lines) tend to exceed those of our parameterization (orange lines) in most of the analyzed cases. Of course, one can easily reduce this error by increasing the highest degree of polynomials considered in the parameterization by Ghan et al. (2001), which is, however, associated with increasing computational costs. With polynomials up to degree 4, the parameterization by Ghan et al. (2001) is, in fact, about 17% faster than our parameterization (tested with 10^6 calls of each parameterization). When polynomials up to degree 5 are used, this advantage decreases to 2%. For polynomials up to degree 6, our parameterization is 9% faster.

All in all, this comparison shows that the results of our new parameterization generally agree with the previous approach by Ghan et al. (2001). At similar computational costs, the new parameterization even enables an improved representation of the interstitial aerosol extinction when a large fraction of aerosol particles is activated into cloud droplets.

b. Parcel simulations

We will continue our verification exercise with simple parcel simulations. The parcel is initially subsaturated, with a temperature $T = 288.3$ K, water vapor mixing ratio $q_v = 9.45$ g kg^{-1}, hydrostatic pressure $p = 1017.8$ hPa, and a relative humidity of about 80%. The parcel is lifted with a constant vertical velocity w until a cloud forms. Then, the parcel is allowed to rise for an additional 800 m, covering the typical range of stratocumulus cloud depths (e.g., Wood 2012).

While one could use a (standard) bulk or bin microphysical model here, the parcel model is coupled to a highly detailed Lagrangian cloud microphysics scheme. This scheme allows one to prescribe and predict the evolution of the entire hydrometeor distribution in the required detail, in particular the changes in the interstitial aerosol mode that are often not covered in bulk or bin microphysical models. The Lagrangian approach is similar to Hoffmann and Feingold (2021), with further details available in Hoffmann et al. (2015). Briefly, the hydrometeor distribution is represented using 800 computational particles. A dry aerosol radius is assigned to each particle using a random generator that follows the assumed lognormal aerosol distribution. The dry aerosol is assumed to consist of sodium chloride, NaCl. The initial radius of each liquid particle is adjusted to its thermodynamic environment, and develops freely once the simulation has started. In total, 10 000 simulations are conducted, with a randomly varied w between 0.1 and 0.8 m s^{-1}, N_a between 100 and 10 000 cm^{-3}, $r_{a,\mathrm{mean}}$ between 25 and 100 nm, and σ_s between 1.1 and 2.0.

The extinction $\beta_{\mathrm{ext},a}$ is calculated using the parameterization (7), as well as and the exact Mie scattering code by Wiscombe (1980) that provided Q_{ext} to solve the integral (2). It is important to note that $\beta_{\mathrm{ext},a}$ is only determined in the cloud layer. The model is run with an internal time step of 0.1 s, while the data are written out every 1 s.

In the Lagrangian cloud model, $r_{a,\mathrm{crit}}$ cannot be (directly) determined from (10) to (12) because the activation process is explicitly represented and not parameterized. To distinguish between interstitial aerosols and cloud droplets, $r_{a,\mathrm{crit}}$ is diagnosed by comparing the liquid radius r of each simulated particle to its critical radius for activation,

$$r_{\mathrm{crit}} = \left(3\,\frac{\mathrm{br}_a^3}{A}\right)^{1/2}, \tag{17}$$

which can be derived from Köhler theory. With this comparison, we find $r_{a,\mathrm{crit}}$ as the largest r_a of all particles with $r < r_{\mathrm{crit}}$, i.e., the interstitial aerosol mode. As initially suggested by Nenes et al. (2001), we consider all particles with an r larger than $r_{\mathrm{crit}} = (3\mathrm{br}_{a,\mathrm{crit}}^3/A)^{1/2}$ as activated. This approach avoids the misclassification of droplets growing from large aerosol particles as unactivated, as these particles are often smaller than their individual r_{crit} although they behave like regular droplets (e.g., Hoffmann 2017). With this definition, we can diagnose N_c from our simulations, which is then used in (10) to (12) to back-calculate a $r_{a,\mathrm{crit}}$. Unsurprisingly, the back-calculated $r_{a,\mathrm{crit}}$ is very similar to the initially diagnosed $r_{a,\mathrm{crit}}$, while it varies due to the inherent limitations of representing a smooth hydrometeor distribution with a finite number of computational particles (not shown).

Figure 3a shows that the variability of the Mie reference $\beta_{\mathrm{ext},a}$ is predicted successfully by our parameterization, as indicated by a relatively high R value of 0.928. Generally, the parameterization is more likely to underestimate $\beta_{\mathrm{ext},a}$ than to overestimate it. As expected from the discussion of Fig. 2, the parameterization becomes most successful when $r_{a,\mathrm{mean}}$ is large, while small $r_{a,\mathrm{mean}}$ tend to overestimate $\beta_{\mathrm{ext},a}$ (Fig. 3c). Similarly, small σ_a result in an underestimated $\beta_{\mathrm{ext},a}$ (Fig. 3d). Note that these deviations are tied to the parameterization's capability of representing Mie scattering. Additionally, the parcel simulations also reveal some microphysical impacts on the parameterization's performance. Most prominently, the parameterization underestimates $\beta_{\mathrm{ext},a}$ in the first tens of

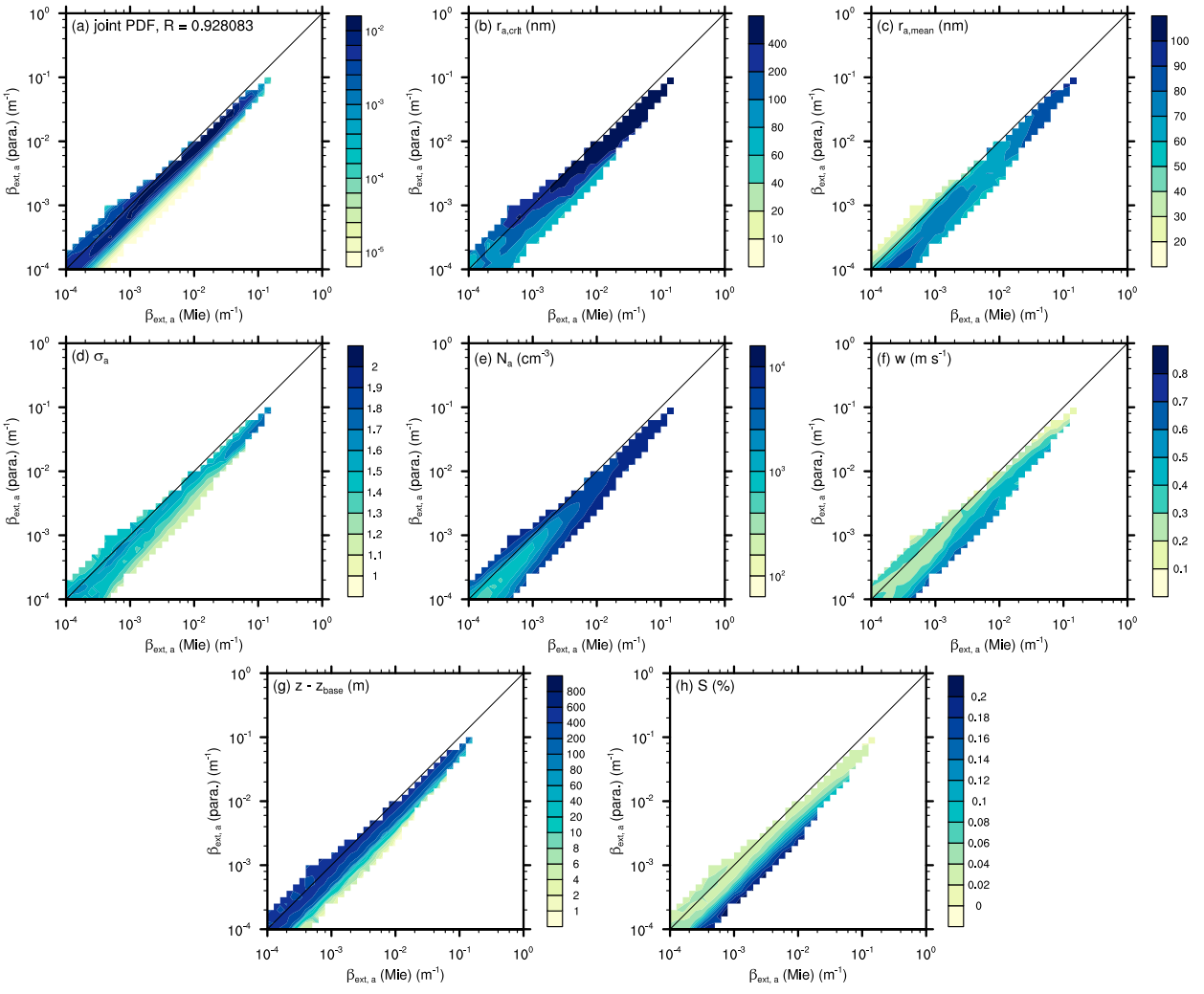

FIG. 3. Scatterplots of the parameterized $\beta_{ext,a}$ (ordinate) against the Mie $\beta_{ext,a}$ (abscissa), showing (a) the joint probability density distribution (PDF), (b) $r_{a,crit}$, (c) $r_{a,mean}$, (d) σ_a, (e) N_a, (f) w, and (g) height above cloud base, and (h) S derived from parcel simulations.

meters above cloud base (Fig. 3g), where high vertical velocities (Fig. 3f) and comparably small cloud droplets result in high supersaturations S (Fig. 3h), with commensurately larger radii than assumed in (5).

For large $r_{a,crit}$, i.e., when a large fraction of the aerosol is in the interstitial aerosol mode, the parameterization behaves best (Fig. 3b). This is because the largest and hence strongest scattering particles are within the geometric scattering limit, for which the parameterization's deviation from the Mie reference $\beta_{ext,a}$ is the lowest (cf. Fig. 1). Figures 3e and 3f indicate that these large values of $r_{a,crit}$ are reached when activation is inefficient, either due to high aerosol concentrations or small vertical velocities. This already indicates that an assessment of MCB should not neglect the contribution of interstitial aerosol to the cloud optical properties in regimes dominated by low vertical velocities. We will continue discussing this aspect in the context of MCB in section 4 below.

Note that we have focused here on the variability of $\beta_{ext,a} > 10^{-4}\ m^{-1}$. While the parameterization also captures smaller $\beta_{ext,a}$ well, any deviations are of a commensurately smaller importance for the cloud optical properties and are therefore not discussed here.

c. *Large-eddy simulations*

As a next step, we apply the parameterization to a more realistic setup, using the large-eddy simulation (LES) model SAM (Khairoutdinov and Randall 2003), coupled to the aforementioned Lagrangian cloud model. Again, we could use a (standard) bulk or bin microphysical model here, but we want to use the Lagrangian microphysics to verify the validity of our assumptions on the changes in the interstitial aerosol mode. We simulate the LES case based on the first research flight of DYCOMS-II (Stevens 2005), with a grid resolution of $35 \times 35 \times 5\ m^3$ and $96 \times 96 \times 256$ grid points in both of the horizontal, and the vertical directions, respectively. Forty computational particles are used per grid box, and results are always averaged over nine horizontally adjacent grid boxes to improve the model's ability to represent a smooth hydrometeor

distribution. A model time step of 0.5 s is applied over a simulation period of 4 h. Three-dimensional snapshots are obtained every 10 min from the entire domain, from which only those from the last hour of the simulation are analyzed in the following.

The aerosol size distribution is based on Connolly et al. (2014), using a trimodal lognormal background distribution with $r_{a,\mathrm{mean}} = (9, 19.5, 77\ \mathrm{nm})$, $\sigma_a = (1.416, 1.425, 1.592)$, and $N_a = (46.46, 153.42, 166.77\ \mathrm{cm}^{-3})$, representing a typical stratocumulus environment potentially targeted during MCB. A typical MCB aerosol mode is added with $r_{a,\mathrm{mean}} = 50$ nm, $\sigma_a = 2$, and $N_a = 1000\ \mathrm{cm}^{-3}$. As before, all aerosol is assumed to consist of sodium chloride, NaCl, and the dry radii are assigned using a random generator. We follow the same procedure to determine N_c and $r_{a,\mathrm{crit}}$ outlined above.

Similar to the parcel simulations, the parameterization represents the variability of $\beta_{\mathrm{ext},a}$ with an R value of 0.933 successfully (Fig. 4a). The parameterization is most successful when large values of $\beta_{\mathrm{ext},a}$ are predicted, i.e., when $r_{a,\mathrm{crit}}$ requires the parameterization of large fractions of the aerosol spectrum. This is most likely close to the cloud base (Fig. 4d), at almost saturated conditions (Fig. 4e), and at high adiabaticities (Fig. 4d), which are defined as the ratio of the actual cloud liquid water mixing ratio to its adiabatic value, $q_c/q_{c,\mathrm{aida}}$.

Deviations from the Mie reference $\beta_{\mathrm{ext},a}$ are associated with the large-scale dynamics of stratocumulus-topped boundary layers (e.g., Lilly 1968; Yamaguchi and Randall 2008; Hoffmann et al. 2020): The so-called large-eddy circulation, driven by the emission of longwave radiation, spans the entire boundary layer and transports air from the surface through the cloud base to the cloud top almost adiabatically. At the cloud top, free-tropospheric air is entrained and subsequently mixed with the cloud within the downward branches of the large-eddy circulation, causing subsaturated environments. Associated with these up- and downdrafts are over and underestimations of $\beta_{\mathrm{ext},a}$ that are explained next.

The parameterization typically overestimates $\beta_{\mathrm{ext},a}$ in updrafts (Fig. 4b) and in almost adiabatic regions of the cloud (Fig. 4d). The reason is interstitial aerosol particles that do not equilibrate immediately after entering the cloud. This is usually the case for particles growing from dry aerosol radii larger than 100 nm, while smaller particles may equilibrate more quickly (Ivanova et al. 1977). In the parcel simulations discussed above, this effect was offset by higher supersaturations caused by stronger updrafts, while this LES exhibits much lower supersaturations (Fig. 4e), making the interstitial aerosol more susceptible to this effect.

Downdrafts, on the other hand, tend to create environments in which $\beta_{\mathrm{ext},a}$ is underestimated by the parameterization (Fig. 4b). Because entrainment affects this region of the state space, as indicated by low adiabaticities (Fig. 4d) and the prevailing subsaturations (Fig. 4e), many interstitial particles are most likely recently deactivated cloud droplets that are currently evaporating to their equilibrium size, as previously observed by Feingold and Morley (2003). Accordingly, the interstitial aerosol particles are larger than the equilibrium size (5) assumed in the parameterization, and hence $\beta_{\mathrm{ext},a}$ is underestimated. Interestingly, there is also a region in the state space where the parameterization overestimates $\beta_{\mathrm{ext},a}$ in downdrafts (parameterized $\beta_{\mathrm{ext},a} > 10^{-4}$). Because this region is located at the cloud top of around 200 m above cloud base (Fig. 4f), entrainment might just recently have engulfed free-tropospheric aerosol. As the air is subsaturated (Fig. 4e), these particles will assume a much smaller size than the equilibrium size (5), or grow more slowly toward (5), similar to the updraft regions of the state space above.

Comparing $q_c/q_{c,\mathrm{aida}}$ (Fig. 4d) to Fig. 4a indicates that most data points are in subadiabatic regions of the cloud, i.e., parts that are affected by dilution through entrainment and subsequent evaporation. The fact that the $\beta_{\mathrm{ext},a}$ parameterization captures regions $q_c/q_{c,\mathrm{aida}} > 0.7$ relatively well indicates that although evaporation does not necessarily deactivate droplets containing the smallest aerosol size first, the procedure for determining $r_{a,\mathrm{crit}}$ as the largest unactivated aerosol radius [outlined in (10)–(12)] is useful here, although it is exactly based on the assumption that droplets containing the smallest aerosol sizes deactivate first.

All in all, although the aforementioned deviations of the parameterization from the Mie reference $\beta_{\mathrm{ext},a}$ can be substantial, they only cover a small fraction of the simulated cloud (Fig. 4a) and predominately affect regions in which $\beta_{\mathrm{ext},a}$ is small compared to the extinction by cloud droplets, $\beta_{\mathrm{ext},c}$ (Fig. 4c). Thus, one can conclude that the parameterization performs well when $\beta_{\mathrm{ext},a}$ contributes substantially to the optical properties of the cloud, i.e., $\beta_{\mathrm{ext},a} \approx \beta_{\mathrm{ext},c}$.

The above demonstrated dependency of $\beta_{\mathrm{ext},a}$ on the stratocumulus dynamics already indicates that interstitial aerosol particles can mitigate the negative effects of entrainment on cloud albedo, and it may also help to reduce undesired effects of so-called negative liquid water adjustments, i.e., increased entrainment rates that reduce cloud water in aerosol-laden environments as a result of accelerated evaporation at the cloud top (Wang et al. 2003; Hoffmann and Feingold 2019; Glassmeier et al. 2021). Hoffmann and Feingold (2021) showed that cloud water can be substantially decreased through this effect when the cloud droplet concentration is increased by a few hundred cm^{-3}, as required for successful MCB. Nonetheless, the commensurate increase in the cloud droplet number prevented an overall decrease in cloud albedo in their simulations, which the authors also attributed to the enhanced contribution of interstitial aerosol particles as discussed in more detail in this study. Note that Hoffmann and Feingold (2021) were only able to determine the contribution of interstitial aerosol particles to the cloud albedo by integrating the entire particle size distribution via (2), for which a computationally expensive Lagrangian cloud model had to be applied. Computational costs prohibit the application of this type of model to a wide range of boundary and initial conditions, which would be necessary to assess MCB comprehensively. The new parameterization of $\beta_{\mathrm{ext},a}$ presented here will augment computationally inexpensive cloud models to address these issues more appropriately. In the next section, we will shown when the contribution of $\beta_{\mathrm{ext},a}$ to the cloud optical thickness is important.

4. Application

Now, we determine situations in which $\beta_{\mathrm{ext},a}$ contributes substantially to the cloud optical thickness. For this, we

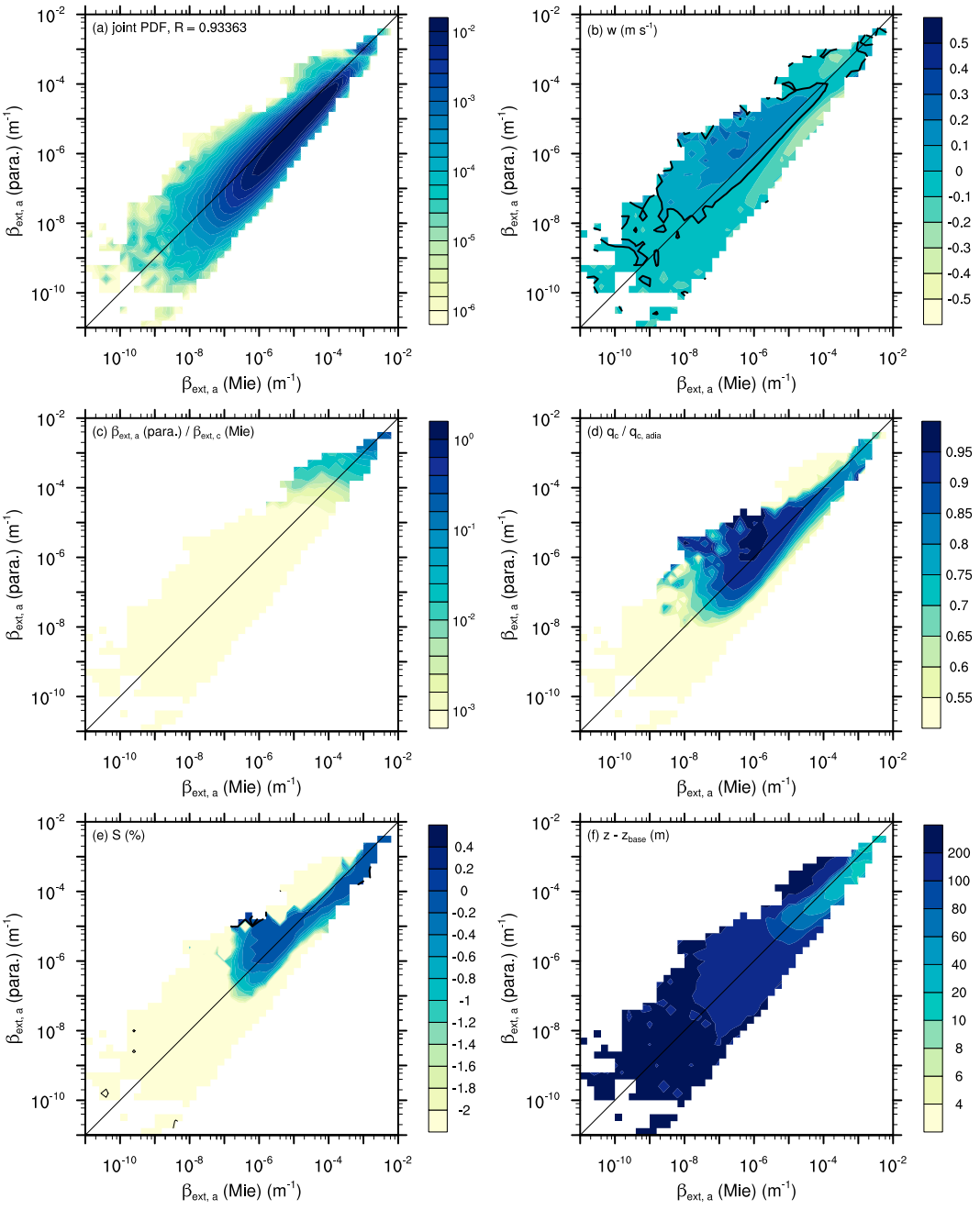

FIG. 4. Scatterplots of the parameterized $\beta_{\text{ext},a}$ (ordinate) against the Mie $\beta_{\text{ext},a}$ (abscissa), showing (a) the joint PDF, (b) w, (c) $\beta_{\text{ext},a}/\beta_{\text{ext},c}$, (d) $q_c/q_{c,\text{adia}}$, (e) S, and (f) height above cloud base derived from an LES. The black line indicates the zero contour for w and S.

apply the same parcel model as used in section 3, and use the same trimodal lognormal background aerosol distribution as in the LES above. Three different MCB cases are presented, all with $\sigma_a = 2$ and $N_a = 1000$ cm^{-3}, as above. We vary $r_{a,\text{mean}}$ from 15 to 25 to 50 nm, covering the range of suggested values in Connolly et al. (2014) and Wood (2021). The vertical velocity w is varied between 0.1 and 0.8 m s^{-1}, covering a realistic range of vertical velocities in stratocumulus clouds (e.g., Wood 2012; Ahola et al. 2022), lifting the parcel 800 m above cloud base. Every setup is simulated 100 times for statistical convergence.

The simulations are presented in Fig. 5, in which each row shows the results for a different seeded $r_{a,\text{mean}}$. The first column of Fig. 5 depicts the liquid water mixing ratio for the aerosol and cloud partition of the particle spectrum, q_a (orange lines) and q_c (green lines), respectively. q_c increases

almost adiabatically with height, and is therefore only negligibly affected by the seeded $r_{a,\mathrm{mean}}$ and w. Because curvature effects limit the growth of the interstitial aerosol particles, q_a assumes an almost constant value above cloud base that, however, varies with $r_{a,\mathrm{mean}}$ and w. The dependency on $r_{a,\mathrm{mean}}$ is caused by the increasing equilibrium radii of larger aerosol particles, while w determines the partitioning into activated and deactivated particles, creating a larger fraction of interstitial aerosol particles when w is low, as shown by the concentration of unactivated particles $N_a' = N_a - N_c$ and the concentration of activated cloud droplets N_c (second column of Fig. 5). While a larger $r_{a,\mathrm{mean}}$ facilitates activation, i.e., a larger N_c for the same w, it is important to note that q_a can even increase when N_a' decreases for larger $r_{a,\mathrm{mean}}$.

The third column of Fig. 5 shows $\beta_{\mathrm{ext},a}$ from Mie calculations (black lines) and the new parameterization (orange lines), as well as the cloud droplet $\beta_{\mathrm{ext},c}$ from the Mie reference (green lines). While $\beta_{\mathrm{ext},c}$ is primarily determined by the change of q_c with height (first column of Fig. 5), it also increases with N_c (second column of Fig. 5) as intended in MCB. Similarly, $\beta_{\mathrm{ext},a}$ increases with N_a' and $r_{a,\mathrm{mean}}$ as expected, indicating more numerous and larger interstitial aerosol particles that scatter more radiation. Note, however, that $\beta_{\mathrm{ext},a} > \beta_{\mathrm{ext},c}$ at cloud base and is only exceeded by $\beta_{\mathrm{ext},c}$ a few tens to one hundred meters above cloud base, required for the comparably small number of cloud droplets to grow sufficiently to exceed $\beta_{\mathrm{ext},a}$. This is analyzed further in the fourth column, where the ratio $\beta_{\mathrm{ext},a}/\beta_{\mathrm{ext},c}$ is depicted. Here, the numerator is derived from Mie calculations (black lines) or the new parameterization (orange lines), while the denominator is always derived from Mie calculations. As expected, $\beta_{\mathrm{ext},a}/\beta_{\mathrm{ext},c}$ decreases with distance from the cloud base, indicating a decreasing impact of the interstitial aerosol on the cloud albedo, confirming Wood (2021) that MCB is only possible when clouds are present, and aerosol particles alone—even in saturated conditions—do not contribute substantially to the cloud albedo. However, for shallower clouds with depths of up to 150 m, the contribution of $\beta_{\mathrm{ext},a}$ can constitute a substantial fraction of up to 0.1 of the total extinction, especially when w is low and the seeded $r_{a,\mathrm{mean}}$ is large. As w and the cloud depth (or more precisely the cloud-top radiative cooling by the emission of longwave radiation that is proportional to the cloud depth) are highly correlated (Zheng et al. 2016; Ahola et al. 2022), larger seeded aerosol particles are to be preferred over smaller aerosol particles when the targeted clouds are shallow or in situations in which shortwave radiation diminishes cloud-top radiative cooling. In this sense, our result support Ahlm et al. (2017), who suggested seeding even larger aerosol particles (up to 220 nm) to increase the global albedo, even in the absence of clouds.

5. Summary and conclusions

Marine cloud brightening (MCB) describes efforts to counteract global warming by the seeding of sea salt aerosol particles that—once activated—increase the number of cloud droplets, cloud albedo, and hence amount of solar radiation reflected back to space (Latham and Smith 1990). However, not all seeded aerosol particles activate, and thus a large fraction of the aerosol remains interstitial, i.e., unactivated aerosol particles among cloud droplets. Quantifying their contribution to the cloud albedo has been computationally challenging since it requires the detailed modeling of the unactivated aerosol size distribution, usually neglected in many types of current cloud models, as well as expensive Mie calculations to determine the scattering properties of these particles. Thus, in this study, we have presented a simple parameterization of the shortwave interstitial aerosol extinction $\beta_{\mathrm{ext},a}$, which—integrated over the cloud layer—can constitute an important contribution to the cloud albedo, especially in typical MCB situations where the number of aerosol particles is substantially increased.

The parameterization is determined analytically assuming that (i) aerosol particles are lognormally distributed, (ii) the extinction efficiency Q_{ext} can be represented by the harmonic mean of Rayleigh scattering and the large particle Mie scattering approximation of Nussenzveig and Wiscombe (1980), and (iii) interstitial aerosol particles assume their saturation equilibrium radius once transported into the cloud. As aerosol distributions are often approximated by a sum of multiple lognormal distributions (Jaenicke 1993), assumption (i) is usually fulfilled. Approximation (ii) was originally proposed by Jung and Kim (2007) for dry aerosol particles, and is extended successfully toward wetted interstitial aerosol particles in this study. Assumption (iii) is often satisfied in aerosol-laden conditions common for MCB, where supersaturations are quickly depleted by the large number of cloud droplets. However, specific microphysical and dynamical conditions can cause environments in which the interstitial aerosol radius deviates from the radius assumed in the parameterization, which will be summarized below.

The parameterization is aimed at cloud microphysical models that do not represent the aerosol mode explicitly, and thus are required to apply an activation parameterization, e.g., Abdul-Razzak and Ghan (2000). These models are predominately two- or more-moment bulk cloud microphysical models (e.g., Morrison et al. 2005; Seifert and Beheng 2006) or even bin cloud model schemes that parameterize activation (e.g., Khain et al. 2015). If the underlying aerosol properties are known (geometric mean and standard deviation, aerosol number concentration) and the cloud droplet concentration is predicted by the cloud model, $\beta_{\mathrm{ext},a}$ can even be deduced in an offline calculation, in which the activation parameterization is inverted analytically to calculate several moments of the truncated interstitial aerosol distribution.

We have evaluated the new parameterization by comparing the parameterized $\beta_{\mathrm{ext},a}$ to a $\beta_{\mathrm{ext},a}$ determined by detailed Lagrangian cloud model simulations (Hoffmann et al. 2015) with full Mie calculations (Wiscombe 1980), using parcel and large-eddy simulations to represent the underlying dynamics. It has been shown that the new parameterization captures the variability of $\beta_{\mathrm{ext},a}$ well, which is indicated by a relatively high R value of about 0.93. In fact, the new parameterization performs especially well when large values of $\beta_{\mathrm{ext},a}$ are predicted, and the interstitial aerosol contributes substantially to the cloud optical thickness.

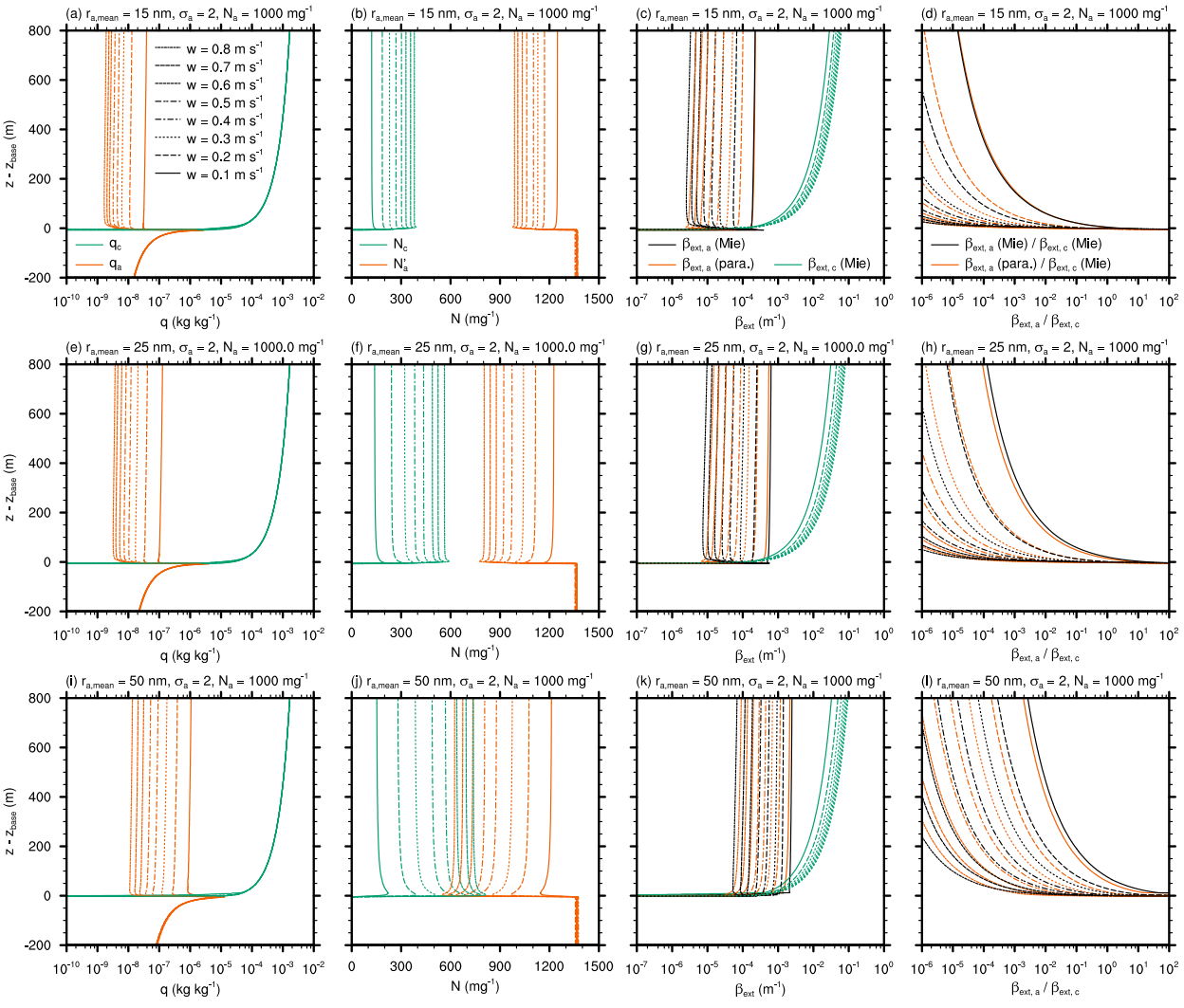

FIG. 5. Vertical profiles of (from left to right) q_a and q_c (orange and green lines, respectively); N'_a and N_c (orange and green lines, respectively); $\beta_{\text{ext},a}$ from Mie theory and parameterization (black and orange lines, respectively) and $\beta_{\text{ext},c}$ from Mie theory (green lines); and $\beta_{\text{ext},a}/\beta_{\text{ext},c}$ from Mie theory and parameterization (black and orange lines, respectively) for different updraft velocities w (line patterns) and different $r_{a,\text{mean}}$ (rows).

Deviations from the Mie reference occur when narrow interstitial aerosol distributions require the accurate representation of Mie oscillations that are not captured by the parameterization (cf. Fig. 1). Further deviations are caused by the interaction of cloud dynamics and the interstitial aerosol distribution: We found $\beta_{\text{ext},a}$ to be underestimated by the parameterization when substantial supersaturations and hence larger interstitial aerosol sizes are produced by strong updrafts at the cloud base (e.g., Mordy 1959). Similarly, $\beta_{\text{ext},a}$ is underestimated in regions of entrainment, where the evaporation of cloud droplets can create interstitial aerosol particles that are (temporarily) larger than assumed in the parameterization (e.g., Feingold and Morley 2003). Conversely, $\beta_{\text{ext},a}$ might be overestimated when entrainment introduces free-tropospheric aerosol that is (temporarily) smaller than assumed in the parameterization. For the analyzed closed-cell stratocumulus, entrainment only affects a small fraction of the cloud, naturally mitigating this error, as indicated by the relatively large R value mentioned above. In open-cell stratocumulus or regular cumulus clouds, in which a larger fraction of the cloud surface participates in environmental mixing, this error might be larger.

While entrainment causes deviations from the parameterization, it is important to note that the adequate consideration of $\beta_{\text{ext},a}$ can also offset some negative impacts of the entrainment-mixing processes on the optical properties of clouds: Since (predominant) inhomogeneous mixing tends to evaporate droplets completely rather than all droplets partially (Baker and Latham 1979; Hoffmann et al. 2019), the decrease in the number of cloud droplets can cause smaller cloud albedos (Chosson et al. 2007; Slawinska et al. 2008). By considering the commensurate increase in the number of scattering

interstitial aerosol particles, the cloud albedo might decrease less than previously anticipated.

In fact, the importance of $\beta_{\text{ext},a}$ for the cloud albedo, (1), can be larger than shown here. While the asymmetry parameter g decreases only moderately for smaller cloud droplets and interstitial aerosol particles, e.g., by 3.5% from 0.85 for an effective radius of 5 μm to 0.82 for 1 μm (e.g., Schwartz et al. 2017), the amount of reflected radiation, which is proportional to $1 - g$, increases by 20% from 0.15 to 0.18 due to the increasing backscatter at smaller particle sizes (e.g., Kokhanovsky 2004). As g is often parameterized as a function of the effective radius (e.g., Hu and Stamnes 1993; Kokhanovsky 2004), the appendix shows a way to determine the effective radius of the entire particle distribution, i.e., the activated cloud droplets and the interstitial aerosol.

Finally, we have analyzed conditions under which the new parameterization has important implications for the optical properties of clouds. For this, we returned to simple parcel simulations but now with a realistic background aerosol distribution for three different MCB cases. We found that especially in shallow clouds (<150 m) with weak updrafts (<0.3 m s^{-1}) the interstitial aerosol contributes substantially to the cloud optical thickness because neither activation nor diffusional growth result in a substantial increase in the extinction by cloud droplets. We showed that in these conditions, larger seeded aerosol particles are useful as they activate more easily, and if not, exhibit larger equilibrium radii in the interstitial aerosol mode, causing a larger $\beta_{\text{ext},a}$. These findings agree qualitatively with Ahlm et al. (2017), who showed that substantially larger seeded aerosol particles can cause substantial MCB, even in the absence of clouds. Nonetheless, the seeding of smaller aerosol particles may be more efficient in the brightening of clouds, as more particles can be created from the same amount of seawater (Connolly et al. 2014; Wood 2021). This is certainly true for stratocumulus that exceed depths of 150 m, in which the cloud albedo is, in fact, primarily caused by cloud droplets. While many stratocumulus exceed depths of 150 m (e.g., Wood 2012), a rigorous MCB assessment also requires consideration of the meteorological conditions that can result in shallower stratocumulus decks. As it might not be possible to eschew these (unfavorable) conditions, e.g., because the relocation of spraying apparatus is too slow or too expensive, localized seeding of larger aerosol particles to optimize the contribution of interstitial aerosol to the cloud albedo may be advisable. To understand this more clearly, simulations that cover larger spatial domains and longer time spans are required. To enable such simulations, more efficient cloud microphysical models than the Lagrangian approach used here are necessary (cf. Hoffmann and Feingold 2021). Thus, parameterizations like the expression presented for $\beta_{\text{ext},a}$ can be a meaningful addition to computationally more efficient cloud microphysical models to consider processes that have not been included before, enabling more realistic assessments of MCB in the future.

Acknowledgments. FH appreciates support from the Emmy Noether program of the German Research Foundation (DFG) under Grant HO 6588/1-1. GF acknowledges support from an Earth's Radiation Budget grant, NOAA CPO Climate and CI 03-01-07-001. Marat Khairoutdinov graciously provided the SAM model.

Data availability statement. The data that support the findings of this study, as well as the applied Lagrangian cloud microphysical model, are available from the corresponding author upon request.

APPENDIX

The Total Effective Radius and the Asymmetry Parameter g

To calculate the cloud albedo A_c, (1), from the cloud optical thickness τ_c, (2), one needs to prescribe the degree of forward scattering by the asymmetry parameter g. For cloud droplets interacting with shortwave radiation, $g \approx 0.85$. However, g decreases for smaller particles, such as interstitial aerosol, indicating a larger degree of backward scattering and hence a larger A_c.

Hu and Stamnes (1993) and Kokhanovsky (2004) showed that g can be parameterized by the effective radius

$$r_{\text{eff}} = \frac{\int_0^\infty r^3 n(r) dr}{\int_0^\infty r^2 n(r) dr} = r_{\text{eff},a} \frac{M_{a,2}}{M_{a,2} + M_{c,2}} + r_{\text{eff},c} \frac{M_{c,2}}{M_{a,2} + M_{c,2}}, \tag{A1}$$

where r is the radius of the droplet or interstitial aerosol particle, $n(r)$ the corresponding distribution function, and $M_{a,2}$ and $M_{c,2}$ the second moment of the interstitial aerosol particles and cloud droplets, respectively. The effective radius of the interstitial aerosol particles can be determined as

$$r_{\text{eff},a} = \frac{M_{a,3}}{M_{a,2}}, \tag{A2}$$

using the moments of the interstitial aerosol size distribution $M_{a,k}$ given in (8). As stated above, the cloud droplet effective radius $r_{\text{eff},c}$ can be expressed as a function of the volume mean radius,

$$r_{\text{eff},c} = k_{\text{FR12}} \left(\frac{q_c}{\frac{4}{3} \pi \rho_l N_c} \right)^{1/3} = \frac{M_{c,3}}{M_{c,2}}, \tag{A3}$$

with q_c the cloud water content, N_c the cloud droplet number concentration, ρ_l the mass density of water, and $k_{\text{FR12}} \approx 1.08$ an empirical constant of proportionality that depends on the width of the droplet size distribution. With $M_{c,3} = q_c/(4\pi\rho_l/3)$, it follows that $M_{c,2} = M_{c,3}/r_{\text{eff},c}$.

This definition of r_{eff} can now be used in, e.g., the approximation of g by Kokhanovsky (2004), who showed that for water particles

$$g = 0.85 - \frac{0.5}{(2\pi r_{\text{eff}}/\lambda)^{2/3}}, \tag{A4}$$

where λ is the wavelength.

REFERENCES

Abdul-Razzak, H., and S. J. Ghan, 2000: A parameterization of aerosol activation: 2. Multiple aerosol types. *J. Geophys. Res.*, **105**, 6837–6844, https://doi.org/10.1029/1999JD901161.

——, and ——, 2002: A parameterization of aerosol activation 3. Sectional representation. *J. Geophys. Res.*, **107**, 4026, https://doi.org/10.1029/2001JD000483.

——, ——, and C. Rivera-Carpio, 1998: A parameterization of aerosol activation: 1. Single aerosol type. *J. Geophys. Res.*, **103**, 6123–6131, https://doi.org/10.1029/97JD03735.

Ahlm, L., A. Jones, C. W. Stjern, H. Muri, B. Kravitz, and J. E. Kristjánsson, 2017: Marine cloud brightening—As effective without clouds. *Atmos. Chem. Phys.*, **17**, 13 071–13 087, https://doi.org/10.5194/acp-17-13071-2017.

Ahola, J., and Coauthors, 2022: Parameterising cloud base updraft velocity of marine stratocumuli. *Atmos. Chem. Phys.*, **22**, 4523–4537, https://doi.org/10.5194/acp-22-4523-2022.

Baker, M. B., and J. Latham, 1979: The evolution of droplet spectra and the rate of production of embryonic raindrops in small cumulus clouds. *J. Atmos. Sci.*, **36**, 1612–1615, https://doi.org/10.1175/1520-0469(1979)036<1612:TEODSA>2.0.CO;2.

Chosson, F., J.-L. Brenguier, and L. Schüller, 2007: Entrainment-mixing and radiative transfer simulation in boundary layer clouds. *J. Atmos. Sci.*, **64**, 2670–2682, https://doi.org/10.1175/JAS3975.1.

Connolly, P. J., G. B. McFiggans, R. Wood, and A. Tsiamis, 2014: Factors determining the most efficient spray distribution for marine cloud brightening. *Philos. Trans. Roy. Soc.*, **A372**, 20140056, https://doi.org/10.1098/rsta.2014.0056.

Cooper, G., J. Foster, L. Galbraith, S. Jain, A. Neukermans, and B. Ormond, 2014: Preliminary results for salt aerosol production intended for marine cloud brightening, using effervescent spray atomization. *Philos. Trans. Roy. Soc.*, **A372**, 20140055, https://doi.org/10.1098/rsta.2014.0055.

Diamond, M. S., A. Gettelman, M. D. Lebsock, A. McComiskey, L. M. Russell, R. Wood, and G. Feingold, 2022: To assess marine cloud brightening's technical feasibility, we need to know what to study—And when to stop. *Proc. Natl. Acad. Sci. USA*, **119**, e2118379119, https://doi.org/10.1073/pnas.2118379119.

Feingold, G., and Z. Levin, 1986: The lognormal fit to raindrop spectra from frontal convective clouds in Israel. *J. Climate Appl. Meteor.*, **25**, 1346–1363, https://doi.org/10.1175/1520-0450(1986)025<1346:TLFTRS>2.0.CO;2.

——, and B. Morley, 2003: Aerosol hygroscopic properties as measured by lidar and comparison with in situ measurements. *J. Geophys. Res.*, **108**, 4327, https://doi.org/10.1029/2002JD002842.

Freud, E., and D. Rosenfeld, 2012: Linear relation between convective cloud drop number concentration and depth for rain initiation. *J. Geophys. Res.*, **117**, D02207, https://doi.org/10.1029/2011JD016457.

Ghan, S. J., and R. A. Zaveri, 2007: Parameterization of optical properties for hydrated internally mixed aerosol. *J. Geophys. Res.*, **112**, D10201, https://doi.org/10.1029/2006JD007927.

——, N. Laulainen, R. Easter, R. Wagener, S. Nemesure, E. Chapman, Y. Zhang, and R. Leung, 2001: Evaluation of aerosol direct radiative forcing in mirage. *J. Geophys. Res.*, **106**, 5295–5316, https://doi.org/10.1029/2000JD900502.

Glassmeier, F., F. Hoffmann, J. S. Johnson, T. Yamaguchi, K. S. Carslaw, and G. Feingold, 2021: Aerosol-cloud-climate cooling overestimated by ship-track data. *Science*, **371**, 485–489, https://doi.org/10.1126/science.abd3980.

Gulev, S., and Coauthors, 2021: Changing state of the climate system. *Climate Change 2021: The Physical Science Basis*, Cambridge University Press, 287–422.

Hale, G. M., and M. R. Querry, 1973: Optical constants of water in the 200-nm to 200-μm wavelength region. *Appl. Opt.*, **12**, 555–563, https://doi.org/10.1364/AO.12.000555.

Hoffmann, F., 2017: On the limits of Köhler activation theory: How do collision and coalescence affect the activation of aerosols? *Atmos. Chem. Phys.*, **17**, 8343–8356, https://doi.org/10.5194/acp-17-8343-2017.

——, and G. Feingold, 2019: Entrainment and mixing in stratocumulus: Effects of a new explicit subgrid-scale scheme for large-eddy simulations with particle-based microphysics. *J. Atmos. Sci.*, **76**, 1955–1973, https://doi.org/10.1175/JAS-D-18-0318.1.

——, and ——, 2021: Cloud microphysical implications for marine cloud brightening: The importance of the seeded particle size distribution. *J. Atmos. Sci.*, **78**, 3247–3262, https://doi.org/10.1175/JAS-D-21-0077.1.

——, S. Raasch, and Y. Noh, 2015: Entrainment of aerosols and their activation in a shallow cumulus cloud studied with a coupled LCM–LES approach. *Atmos. Res.*, **156**, 43–57, https://doi.org/10.1016/j.atmosres.2014.12.008.

——, T. Yamaguchi, and G. Feingold, 2019: Inhomogeneous mixing in Lagrangian cloud models: Effects on the production of precipitation embryos. *J. Atmos. Sci.*, **76**, 113–133, https://doi.org/10.1175/JAS-D-18-0087.1.

——, F. Glassmeier, T. Yamaguchi, and G. Feingold, 2020: Liquid water path steady states in stratocumulus: Insights from process-level emulation and mixed-layer theory. *J. Atmos. Sci.*, **77**, 2203–2215, https://doi.org/10.1175/JAS-D-19-0241.1.

Hu, Y., and K. Stamnes, 1993: An accurate parameterization of the radiative properties of water clouds suitable for use in climate models. *J. Climate*, **6**, 728–742, https://doi.org/10.1175/1520-0442(1993)006<0728:AAPOTR>2.0.CO;2.

Ivanova, E., Y. Kogan, I. Mazin, and M. Permyakov, 1977: Method of parameterizing the condensation process of droplet growth in numerical models. *Izv. Acad. Sci. USSR Atmos. Oceanic Phys.*, **13**, 821–826.

Jacobson, M. Z., 2005: *Fundamentals of Atmospheric Modeling*. 2nd ed. Cambridge University Press, 829 pp.

Jaenicke, R., 1993: Tropospheric aerosols. *Aerosol–Cloud–Climate Interactions*, P. V. Hobbs, Ed., International Geophysics Series, Vol. 54, Elsevier, 1–31, https://doi.org/10.1016/S0074-6142(08)60210-7.

Jung, C. H., and Y. P. Kim, 2007: Particle extinction coefficient for polydispersed aerosol using a harmonic mean type general approximated solution. *Aerosol Sci. Technol.*, **41**, 994–1001, https://doi.org/10.1080/02786820701644285.

Khain, A., and Coauthors, 2015: Representation of microphysical processes in cloud-resolving models: Spectral (bin) microphysics versus bulk parameterization. *Rev. Geophys.*, **53**, 247–322, https://doi.org/10.1002/2014RG000468.

Khairoutdinov, M. F., and D. A. Randall, 2003: Cloud resolving modeling of the ARM summer 1997 IOP: Model formulation, results, uncertainties, and sensitivities. *J. Atmos. Sci.*, **60**, 607–625, https://doi.org/10.1175/1520-0469(2003)060<0607:CRMOTA>2.0.CO;2.

Khvorostyanov, V. I., and J. A. Curry, 1999: A simple analytical model of aerosol properties with account for hygroscopic

growth: 2. Scattering and absorption coefficients. *J. Geophys. Res.*, **104**, 2163–2174, https://doi.org/10.1029/98JD02687.

——, and ——, 2006: Aerosol size spectra and CCN activity spectra: Reconciling the lognormal, algebraic, and power laws. *J. Geophys. Res.*, **111**, D12202, https://doi.org/10.1029/2005JD006532.

——, and ——, 2007: Refinements to the Köhler's theory of aerosol equilibrium radii, size spectra, and droplet activation: Effects of humidity and insoluble fraction. *J. Geophys. Res.*, **112**, D05206, https://doi.org/10.1029/2006JD007672.

Köhler, H., 1936: The nucleus in and the growth of hygroscopic droplets. *Trans. Faraday Soc.*, **32**, 1152–1161, https://doi.org/10.1039/TF9363201152.

Kokhanovsky, A., 2004: Optical properties of terrestrial clouds. *Earth-Sci. Rev.*, **64**, 189–241, https://doi.org/10.1016/S0012-8252(03)00042-4.

Latham, J., and M. H. Smith, 1990: Effect on global warming of wind-dependent aerosol generation at the ocean surface. *Nature*, **347**, 372–373, https://doi.org/10.1038/347372a0.

——, and Coauthors, 2012: Marine cloud brightening. *Philos. Trans. Roy. Soc.*, **A370**, 4217–4262, https://doi.org/10.1098/rsta.2012.0086.

Lilly, D. K., 1968: Models of cloud-topped mixed layers under a strong inversion. *Quart. J. Roy. Meteor. Soc.*, **94**, 292–309, https://doi.org/10.1002/qj.49709440106.

Liu, X., and Coauthors, 2012: Toward a minimal representation of aerosols in climate models: Description and evaluation in the Community Atmosphere Model CAM5. *Geosci. Model Dev.*, **5**, 709–739, https://doi.org/10.5194/gmd-5-709-2012.

Meador, W. E., and W. R. Weaver, 1980: Two-stream approximations to radiative transfer in planetary atmospheres: A unified description of existing methods and a new improvement. *J. Atmos. Sci.*, **37**, 630–643, https://doi.org/10.1175/1520-0469(1980)037<0630:TSATRT>2.0.CO;2.

Mitchell, D. L., 2000: Parameterization of the Mie extinction and absorption coefficients for water clouds. *J. Atmos. Sci.*, **57**, 1311–1326, https://doi.org/10.1175/1520-0469(2000)057<1311:POTMEA>2.0.CO;2.

Mordy, W., 1959: Computations of the growth by condensation of a population of cloud droplets. *Tellus*, **11**, 16–44, https://doi.org/10.1111/j.2153-3490.1959.tb00003.x.

Morrison, H., J. A. Curry, and V. I. Khvorostyanov, 2005: A new double-moment microphysics parameterization for application in cloud and climate models. Part I: Description. *J. Atmos. Sci.*, **62**, 1665–1677, https://doi.org/10.1175/JAS3446.1.

Nenes, A., S. Ghan, H. Abdul-Razzak, P. Y. Chuang, and J. H. Seinfeld, 2001: Kinetic limitations on cloud droplet formation and impact on cloud albedo. *Tellus*, **53B**, 133–149, https://doi.org/10.3402/tellusb.v53i2.16569.

Nussenzveig, H. M., and W. J. Wiscombe, 1980: Efficiency factors in Mie scattering. *Phys. Rev. Lett.*, **45**, 1490–1494, https://doi.org/10.1103/PhysRevLett.45.1490.

Press, W. H., S. A. Teukolsky, W. T. Vetterling, and B. P. Flannery, 1996: *Numerical Recipes in Fortran 90: The Art of Parallel Scientific Computing*. 2nd ed. Cambridge University Press, 1495 pp.

Salter, S., G. Sortino, and J. Latham, 2008: Sea-going hardware for the cloud albedo method of reversing global warming. *Philos. Trans. Roy. Soc.*, **A366**, 3989–4006, https://doi.org/10.1098/rsta.2008.0136.

Schwartz, S. E., D. Huang, and D. V. Vladutescu, 2017: High-resolution photography of clouds from the surface: Retrieval of optical depth of thin clouds down to centimeter scales. *J. Geophys. Res. Atmos.*, **122**, 2898–2928, https://doi.org/10.1002/2016JD025384.

Sedunov, Y. S., 1974: *Physics of Drop Formation in the Atmosphere*. John Wiley and Sons, 244 pp.

Seifert, A., and K. D. Beheng, 2006: A two-moment cloud microphysics parameterization for mixed-phase clouds. Part 1: Model description. *Meteor. Atmos. Phys.*, **92**, 45–66, https://doi.org/10.1007/s00703-005-0112-4.

Shettle, E. P., and R. W. Fenn, 1979: Models for the aerosols of the lower atmosphere and the effects of humidity variations on their optical properties. Air Force Geophysics Laboratory Rep. 214, 94 pp.

Slawinska, J., W. W. Grabowski, H. Pawlowska, and A. A. Wyszogrodzki, 2008: Optical properties of shallow convective clouds diagnosed from a bulk-microphysics large-eddy simulation. *J. Climate*, **21**, 1639–1647, https://doi.org/10.1175/2007JCLI1820.1.

Stevens, B., 2005: Atmospheric moist convection. *Annu. Rev. Earth Planet. Sci.*, **33**, 605–643, https://doi.org/10.1146/annurev.earth.33.092203.122658.

Tang, I. N., 1997: Thermodynamic and optical properties of mixed-salt aerosols of atmospheric importance. *J. Geophys. Res.*, **102**, 1883–1893, https://doi.org/10.1029/96JD03085.

Twomey, S., 1974: Pollution and the planetary albedo. *Atmos. Environ.*, **8**, 1251–1256, https://doi.org/10.1016/0004-6981(74)90004-3.

Vaughan, N. E., and T. M. Lenton, 2011: A review of climate geoengineering proposals. *Climatic Change*, **109**, 745–790, https://doi.org/10.1007/s10584-011-0027-7.

Victor, D., D. Zhou, E. Ahmed, P. K. Dadhich, J. Olivier, H.-H. Rogner, K. Sheikho, and M. Yamaguchi, 2014: Introductory chapter. *Climate Change 2014: Mitigation of Climate Change*, O. Edenhofer, et al., Eds., Cambridge University Press, 111–150.

Von der Emde, K., and U. Wacker, 1993: Comments on the relationships between aerosol spectra, equilibrium drop size spectra, and CCN spectra. *Beitr. Phys. Atmos.*, **66**, 157–162, http://pascal-francis.inist.fr/vibad/index.php?action=getRecordDetail&idt=4021314.

Wang, S., Q. Wang, and G. Feingold, 2003: Turbulence, condensation, and liquid water transport in numerically simulated nonprecipitating stratocumulus clouds. *J. Atmos. Sci.*, **60**, 262–278, https://doi.org/10.1175/1520-0469(2003)060<0262:TCALWT>2.0.CO;2.

Wiscombe, W. J., 1980: Improved Mie scattering algorithms. *Appl. Opt.*, **19**, 1505–1509, https://doi.org/10.1364/AO.19.001505.

Wood, R., 2012: Stratocumulus clouds. *Mon. Wea. Rev.*, **140**, 2373–2423, https://doi.org/10.1175/MWR-D-11-00121.1.

——, 2021: Assessing the potential efficacy of marine cloud brightening for cooling Earth using a simple heuristic model. *Atmos. Chem. Phys.*, **21**, 14 507–14 533, https://doi.org/10.5194/acp-21-14507-2021.

Yamaguchi, T., and D. A. Randall, 2008: Large-eddy simulation of evaporatively driven entrainment in cloud-topped mixed layers. *J. Atmos. Sci.*, **65**, 1481–1504, https://doi.org/10.1175/2007JAS2438.1.

Zheng, Y., D. Rosenfeld, and Z. Li, 2016: Quantifying cloud base updraft speeds of marine stratocumulus from cloud top radiative cooling. *Geophys. Res. Lett.*, **43**, 11 407–11 413, https://doi.org/10.1002/2016GL071185.